

# Passivation Analysis of the Emitter and Selective Back Surface Field of Silicon Solar Cells

Ricardo A. Z. Razera and Henri Boudinov  
PGMICRO

Universidade Federal do Rio Grande do Sul  
Porto Alegre, Brazil

Emails: ricardo.razera@inf.ufrgs.br and henry@if.ufrgs.br

Izete Zanesco and Adriano Moehlecke

Faculty of Physics

Pontifícia Universidade Católica do Rio Grande do Sul  
Porto Alegre, Brazil

Emails: izete@pucrs.br and moehleck@pucrs.br

**Abstract**—In this work the high-quality passivation of p-type Si solar cells with a boron-aluminum selective back surface field (BSF) and dry thermal  $\text{SiO}_2$  layers on both surfaces is analyzed comparing the internal quantum efficiency (IQE) and the current-voltage parameters. This structure may be a viable substitute for the industry's standard solar cell, which has to be reconsidered when faced with the bowing problem. We observed that increasing oxidation temperature decreases IQE for short wavelengths (400 nm), while for long wavelengths (1000 nm) the IQE increases for temperatures lower than 860 °C. The same trend is observed for the solar cells' open circuit voltages, indicating that rear surface passivation increases for thicker oxides. The short-circuit current density was affected by the higher reflectance caused by the  $\text{SiO}_2$  layer. However, by adjusting the  $\text{TiO}_2$  anti-reflective coating thickness we were able to avoid this effect, achieving solar cells with efficiencies up to 16.8 %, which is comparable to the current efficiency of cells with Al-BSF covering the whole back surface. Furthermore, no bowing was observed for this structure.

**Keywords**—Silicon Solar Cells, Passivation, Thermal Silicon Dioxide, Internal Quantum Efficiency

## I. INTRODUCTION

Although the usual passivation technique used in the solar cell industry is a  $\text{SiN}_x$  thin film on the front surface and an aluminum back surface field (BSF) on the rear surface [1], recent trends may lead to a change of this scenario. Specifically, the tendency to use thinner wafers (less than 200  $\mu\text{m}$ ) as substrates leads to bowing effects during the Al paste firing to form the Al-BSF in the whole rear surface [2]. A direct solution to the bowing effect is substituting the rear Al-BSF, which covers the whole area, for an Al grid. But this solution implies that it is necessary to change the rear face passivation method, because the parts that are not coated with Al cannot be left unpassivated. Otherwise, the high surface recombination velocity associated to the dangling bonds of bare silicon surfaces would reduce minority carrier lifetime and solar cell efficiency [3], [4], specially for thinner wafers.

Therefore, different passivation methods, compatible with the industry's standard silicon solar cell, are necessary. For example, this method has to be able to passivate the p<sup>+</sup>-type back surface, because the Al-BSF is located only below the metal grid. This means that, even though it would be convenient for the industry to have the same deposition procedure for both surfaces,  $\text{SiN}_x$  is not recommended for back

surface passivation, because  $\text{SiN}_x$  usually cannot passivate p-type surfaces well enough [5].

For these reasons, silicon solar cells with a B-Al selective BSF but with a different back surface passivation layer are being developed [6], since this structure avoids wafer bowing. Here we show that a thin layer of thermal  $\text{SiO}_2$ , together with the B-BSF, passivates the rear surface even further, increasing efficiency. We choose dry thermal  $\text{SiO}_2$  because its excellence in passivating silicon is well known [7], [8], [9]. In fact, with  $\text{SiO}_2$  it is possible to passivate both n and p-type silicon [9], meaning that we can use it for both front and back surfaces. This allows the use of a single oxidation step to passivate both surfaces, which reduces process cost. The passivation analysis is given here in terms of internal quantum efficiency (IQE) and its comparison with electrical parameters.

## II. METHODS

### A. Solar Cell Process and Oxidation

The structure of the solar cells is shown in Fig. 1 and a diagram showing each step of processing is shown in Fig. 2. With exception of the oxidation step, all other procedures used to manufacture this solar cell were optimized in previous works [9], [10], [11], [12]. The substrate was p-type, solar grade czochralski-Si wafers with resistivity of 1-20  $\Omega\cdot\text{cm}$  and with initial thicknesses of 200  $\mu\text{m}$ . The oxidation was performed with  $\text{O}_2$  and was followed by a 10 minute annealing in  $\text{N}_2$  at the same temperature. Based on previous work [13], we fixed the oxidation time ( $t_{oxi}$ ) at 7 minutes and changed the oxidation temperature ( $T_{oxi}$ ) from 770 °C to 920 °C and then fixed  $T_{oxi}$  at 800 °C and changed  $t_{oxi}$  from 2 to 90 minutes in order to optimize the oxidation step. The  $\text{SiO}_2$  thicknesses ranged from 10 to 80 nm in the phosphorous emitter and from 1 to 14 nm in the B-BSF. For each set of  $T_{oxi}$  and  $t_{oxi}$ , three to five solar cells having a pseudo-square shape and area of 61.58  $\text{cm}^2$  were manufactured. The current-voltage (I-V) curve of all solar cells and the internal quantum efficiency of only the best-performing devices of each  $T_{oxi}$  and  $t_{oxi}$  set were measured.

### B. Internal Quantum Efficiency and Electrical Parameters

The IQE is defined as the ratio of the number of collected photogenerated carriers to the number of absorbed photons by the solar cell. With this definition, an IQE of 100% for a

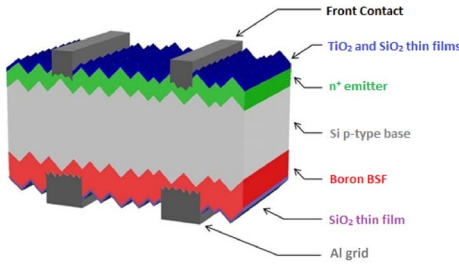


Fig. 1. Silicon solar cell structure with phosphorous emitter and boron/aluminum selective BSF.

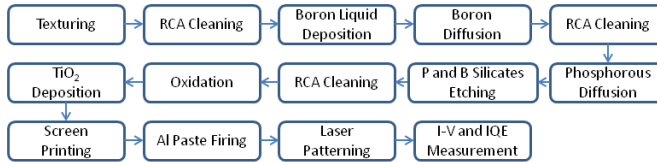


Fig. 2. Process sequence used for solar cells manufacturing.

given wavelength means that all absorbed photons with this wavelength contributed one electron-hole pair to the photocurrent collected in the metallic terminals. IQE was measured using a xenon and a halogen lamp in combination with a monochromator to scan the photocurrent of each solar cell from 300 nm to 1100 nm. The reflectance was measured with an integrating sphere. The IQE can provide information on the passivation of solar cells because different wavelengths have different absorption depths. Short wavelengths are absorbed closer to the illuminated surface and long wavelengths are absorbed deeper into the solar cell. Therefore, the IQE for short (300-500 nm) and long (900-1100 nm) wavelengths can provide information on the front and rear surface passivation, respectively [3]. One has to notice, however, that IQE is also sensitive to the lifetime of minority carriers in the bulk. For low lifetimes, charge carriers produced further into the base have a lower probability of being collected by the emitter. Therefore, low lifetimes reduce IQE for long wavelengths.

The open-circuit voltage ( $V_{oc}$ ) and short-circuit current density ( $J_{sc}$ ) were extracted from the I-V curve, which was measured using AM1.5G spectrum. The irradiance was calibrated to 1000 W/m<sup>2</sup> and the cell temperature was kept at 25°C during the measurements.

### III. RESULTS

Fig. 3 shows the IQE for different oxidation temperatures and with  $t_{oxi}$  fixed at 7 minutes. For ease of visualization, only three of the six curves are shown. Fig. 4 presents the IQE for the particular wavelength values of 400 nm and 1000 nm for all oxidation temperatures. From both Figs. 3 and 4 we see that both front and rear passivation depend on oxidation temperature.

Fig. 4 indicates that the IQE for short wavelengths decreases for increasing oxidation temperatures. This result may be a

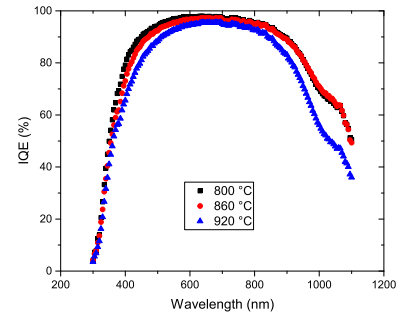


Fig. 3. Internal quantum efficiency (IQE) as a function of wavelength for three different oxidation temperatures. Oxidation time was kept fixed at seven minutes.

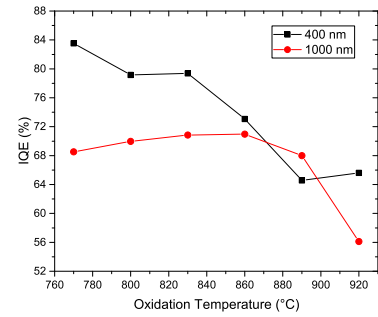


Fig. 4. Internal quantum efficiency (IQE) as a function of oxidation temperatures for wavelengths of 400 nm and 1000 nm.

consequence of the fact that with higher processing temperatures the p-n junction diffuses further into the base, increasing recombination of minority carriers in the emitter. Therefore, the minority carriers excited in this region (which are due to short wavelength photons) have a lower probability of being collected by the deeper p-n junction, lowering IQE for short wavelengths.

On the other hand, for long wavelengths the IQE increases from 770 °C to 860 °C, and then decreases substantially for temperatures higher than 860 °C. The SiO<sub>2</sub> thickness obtained in the B-BSF with 860 °C was about 5 nm. We attribute this increase in IQE to a higher passivation provided by thicker oxides on the boron BSF. However, for high processing temperatures (> 860°C), contamination and defect generation in the sample lower bulk lifetime [14]. The combined effect is that IQE for long wavelengths increases for low oxidation temperatures ( $\leq 860$  °C) but decreases for high temperatures ( $> 860$  °C).

Fig. 5 shows  $J_{sc}$  and  $V_{oc}$  as a function of  $T_{oxi}$ . The  $V_{oc}$  also increases with oxidation temperature for  $T_{oxi} \leq 860$  °C and then decreases for temperatures higher than 860°C. This gives support to our earlier interpretation that for lower processing temperatures the passivation increases because of thicker oxides on the rear surface, but then decreases because

higher temperatures induce a deeper emitter and substrate degradation, which reduce minority carrier lifetime and  $V_{oc}$ . Thus, the higher  $V_{oc}$  values obtained for thicker oxides are a consequence of a higher passivation of the rear surface that contains the boron BSF. On the other hand,  $J_{sc}$  only decreases with increasing  $T_{oxi}$ . This may also be a consequence of a deeper emitter produced at higher temperatures, but can also be attributed to a higher reflectance of the front surface, caused by the  $\text{SiO}_2$  layer between the substrate and the  $\text{TiO}_2$  anti-reflective coating. However, the reflectance can be corrected by depositing a thinner  $\text{TiO}_2$  layer.

Therefore,  $T_{oxi}$  should be as low as possible in order to prevent bulk degradation and a deeper p-n junction, but longer oxidation times are then necessary for thicker oxides and higher passivation of the B-BSF. In fact, as shown in Fig. 6,  $V_{oc}$  stabilizes for  $t_{oxi}$  higher than 45 min, and shows only a little decrease for  $t_{oxi}$  as high as 90 min. We highlight that  $T_{oxi}$  was 800 °C for the curves in Fig. 6. We achieved a  $V_{oc}$  of 604 mV with  $T_{oxi} = 800$  °C and  $t_{oxi} = 45$  min.

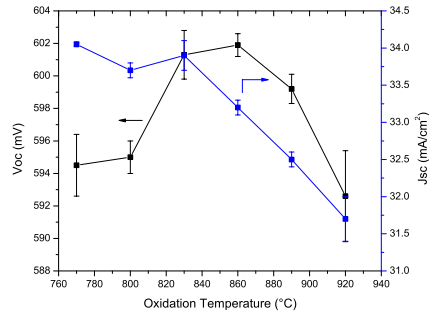


Fig. 5.  $V_{oc}$  and  $J_{sc}$  as a function of oxidation temperature for  $t_{oxi} = 7$  min.

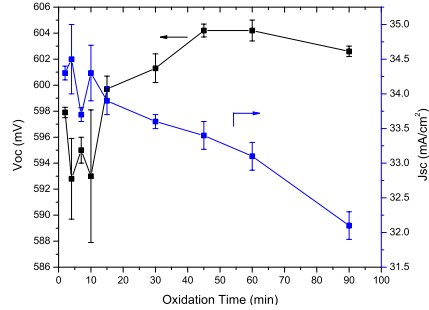


Fig. 6.  $V_{oc}$  and  $J_{sc}$  as a function of oxidation time for  $T_{oxi} = 800$  °C.

From Fig. 6 we can see that increasing  $t_{oxi}$  lowers  $J_{sc}$  substantially, even for the low temperature of 800 °C. This, however, is only a consequence of increased reflectance for thicker oxides in the emitter, as confirmed in the reflectance curves of Fig. 7. In fact, as shown in Fig. 8, we do not observe any appreciable decrease in IQE for short wavelengths and also do not observe substantial reduction in lifetime, since the IQE curves for different oxidation times are slightly changed only for wavelengths higher than about 1000 nm. Thus, the

decrease in  $J_{sc}$  cannot be attributed to a deeper emitter nor to substrate degradation. The highest IQE for long wavelengths occurred for  $t_{oxi} = 45$  min, as for the highest  $V_{oc}$ , confirming that the higher B-BSF passivation increases  $V_{oc}$ .

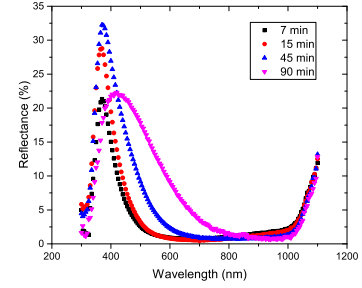


Fig. 7. Reflectance as a function of wavelength for four different oxidation times and  $T_{oxi} = 800$  °C.

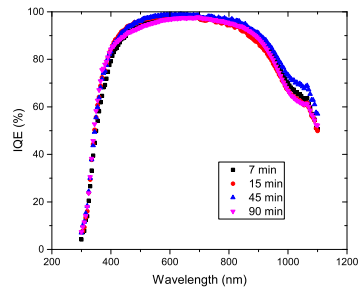


Fig. 8. Internal quantum efficiency (IQE) as a function of wavelength for four different oxidation times and  $T_{oxi} = 800$  °C.

Fig. 9 shows the IQE as a function of oxidation time for short and long wavelengths. We observe that for short wavelengths the IQE was not affected by  $t_{oxi}$ , even though it was influenced by  $T_{oxi}$  as shown in Fig. 4. Moreover, the IQE for long wavelengths confirms that  $t_{oxi} = 45$  min resulted in the best rear surface passivation.

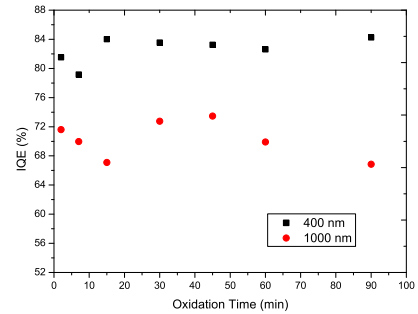


Fig. 9. Internal quantum efficiency (IQE) as a function of oxidation time for 400 and 1000 nm and  $T_{oxi} = 800$  °C.

In order to optimize the reflectance, another batch of solar cells were fabricated with the optimal oxidation of  $T_{oxi} = 800$  °C and  $t_{oxi} = 45$  min, but with the  $\text{TiO}_2$  AR-coating thickness corrected for the presence of a  $\text{SiO}_2$  layer. The rear  $\text{SiO}_2$ , front  $\text{SiO}_2$  and  $\text{TiO}_2$  layers thicknesses were respectively

10 nm, 53 nm and 25 nm. We note that, although only one oxidation step was performed, the oxide thicknesses on each surface were different because the oxidation rate differs for highly doped n and p-type surfaces [15]. With these optimal thicknesses, we measured short-circuit current densities as high as  $36.0 \text{ mA/cm}^2$ , which are about  $3 \text{ mA/cm}^2$  higher than that shown in Fig. 6 for  $t_{oxi} = 45 \text{ min}$ .

The effectiveness of  $\text{SiO}_2$  is further demonstrated in Fig. 10, where a comparison between the IQE of two best-performing solar cells is shown, one with  $\text{SiO}_2$  grown at  $T_{oxi} = 800^\circ\text{C}$  and  $t_{oxi} = 45 \text{ min}$  and  $\text{TiO}_2$  thickness adjusted for the  $\text{SiO}_2$  layer, and the other without oxidation but otherwise equal structure [16]. Both IQE's for short and for long wavelengths are substantially higher with  $\text{SiO}_2$  passivation, indicating that the effective minority carrier lifetime was substantially increased. In fact, the solar cell with  $\text{SiO}_2$  passivation, shown in Fig. 10, compared to the device without  $\text{SiO}_2$ , presented a  $J_{sc}$  increase of  $2.3 \text{ mA/cm}^2$  and a  $V_{oc}$  increase of about  $9 \text{ mV}$ . The fill factor for this solar cell was 77.7% and the efficiency was 16.8%, which is comparable to the cells that have Al-BSF covering the whole back surface, showing that  $\text{SiO}_2$  passivation was effective for solar cells with a B-Al selective BSF. The efficiency of the solar cell without  $\text{SiO}_2$  passivation was 15.1%.

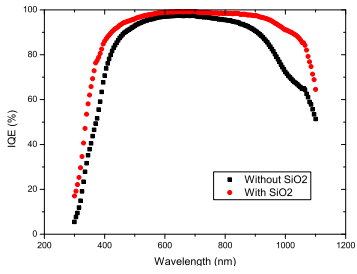


Fig. 10. Internal quantum efficiency (IQE) curves of the best solar cells with and without  $\text{SiO}_2$  but otherwise equal structure.

#### IV. CONCLUSION

In summary, we were able to demonstrate high-quality passivation with thermal  $\text{SiO}_2$  for solar cells with a boron-aluminum selective BSF, achieving efficiencies up to 16.8%. We have also shown that oxidation temperatures higher than  $860^\circ\text{C}$  reduced IQE for both short and long wavelengths and, as a consequence, also reduced  $J_{sc}$  and  $V_{oc}$ . On the other hand, increasing oxide thickness enhances the rear surface passivation, which increases  $V_{oc}$ . The optimal oxidation parameters found were  $T_{oxi} = 800^\circ\text{C}$  and  $t_{oxi} = 45 \text{ min}$ , resulting in 53 nm and 10 nm  $\text{SiO}_2$  layers on the emitter and B-BSF, respectively. We also observed a reduction in  $J_{sc}$  due to an increase in reflectance for thicker oxides on the front side, but were able to correct this effect by reducing the  $\text{TiO}_2$  anti-reflective coating thickness. This work shows that thermal oxidation may be a good candidate for the passivation of both front and rear surfaces in solar cell production.

#### ACKNOWLEDGMENTS

This work was supported by Eletrosul, under the project “Development of Industrial Processes for the Manufacture of Solar Cells with Aluminum Paste and Passivation”, 1110140010, and the National Council of Scientific and Technological Development (CNPq).

#### REFERENCES

- [1] A. Goodrich, P. Hacke, Q. Wang, B. Sopori, R. Margolis, T. James, and M. Woodhouse, “A wafer-based monocrystalline silicon photovoltaics road map: utilizing known technology improvement to opportunities for further reductions in manufacturing costs,” *Solar Energy Materials & Solar Cells*, vol. 114, pp. 110–135, Jan. 2013.
- [2] X. Gu, X. Yu, J. Xu, R. Fan, and D. Yang, “Towards thinner and low bowing silicon solar cells: from the boron and aluminum co-doped back surface field with thinner metallization film,” *Progress in Photovoltaics: Research and Applications*, vol. 21, no. 121, pp. 456–461, Jun. 2013.
- [3] A. G. Aberle, *Crystalline Silicon Solar Cells: Advanced Surface Passivation and Analysis*, 1st ed. Sydney, NSW: Centre for Photovoltaic Engineering, 2000.
- [4] M. A. Green, *Silicon Solar Cells, Advanced Principles & Practice*, 1st ed. Sydney, NSW: Centre for Photovoltaic Devices and Systems, 1995.
- [5] A. G. Aberle, “Surface passivation of crystalline silicon solar cells: a review,” *Progress in Photovoltaics: Research and Applications*, vol. 8, pp. 473–487, Oct. 2000.
- [6] T. Crestani, I. Zanesco, A. Moehlecke, R. A. Z. Razera, J. Aquino, J. C. M. Model, and M. Ly, “Desenvolvimento do campo retrodifusor seletivo de alumínio e boro em células solares de silício,” in *VI Congresso Brasileiro de Energia Solar*, 2016.
- [7] K. Nakamura, K. Okamoto, Y. Kawamoto, Y. Yoshino, and Y. Ohshita, “ $\text{SiO}_2/\text{SiN}_x$  stacking layer for rear surface passivation of perc,” in *Proceedings of the 42nd IEEE Photovoltaic Specialists Conference*. IEEE, 2015.
- [8] R. A. Z. Razera, A. Moehlecke, I. Zanesco, J. Aquino, M. Ly, T. Crestani, and J. C. M. Model, “Análise de processos de oxidação com trans-lc para fabricação de células solares,” in *Acta de la XXXIX Reunión de Trabajo de la Asociación Argentina de Energías Renovables*, vol. 4, 2016, pp. 13–21.
- [9] I. Zanesco, A. Moehlecke, R. A. Z. Razera, J. Aquino, T. Crestani, J. C. M. Model, and M. Ly, “Análise da passivação com  $\text{SiO}_2$  na face posterior e frontal de células solares com campo retrodifusor seletivo,” in *Simpósio Matéria*, 2016, p. 127.
- [10] T. Crestani, I. Zanesco, A. Moehlecke, R. A. Z. Razera, J. Aquino, J. C. M. Model, and M. Ly, “Influência do tempo de difusão de boro no campo retrodifusor seletivo de alumínio e boro em células solares de silício,” in *Acta de la XXXIX Reunión de Trabajo de la Asociación Argentina de Energías Renovables*, vol. 4, 2016, pp. 23–34.
- [11] I. Zanesco and A. Moehlecke, “Desenvolvimento de processos industriais para fabricação de células solares com pasta de Al e passivação,” Eletrosul, Tech. Rep., 2016, p. 383.
- [12] I. Zanesco and A. Moehlecke, “Processo de difusão de dopantes em lâminas de silício para a fabricação de células solares,” BR Patent PI12 030 606, BR 10 2012 030 606 9, Nov. 30, 2012.
- [13] I. Zanesco and A. Moehlecke, “Analysis of the silicon dioxide passivation and forming gas annealing in silicon solar cells.” in *Proceedings of the ISES Solar World Conference*, 2015, pp. 1–9.
- [14] P. Schmidt, “Neutron activation analysis study of the sources of transition group metal contamination in the silicon device manufacturing process.” *Journal of the Electrochemical Society*, vol. 128, no. 3, p. 630, 1981.
- [15] C. P. Ho and J. D. Plummer, “ $\text{Si}/\text{SiO}_2$  interface oxidation kinetics: A physical model for the influence of high substrate doping levels ii. comparison with experiment and discussion.” *Journal of the Electrochemical Society*, vol. 126, no. 9, pp. 1516–1522, 1979.
- [16] J. C. M. Model, A. Moehlecke, I. Zanesco, M. Ly, S. B. Garcia, J. Aquino, T. Crestani, and R. A. Z. Razera, “Comparação das características elétricas de células solares  $n^+np^+$  com filmes antirreflexo de  $\text{TiO}_2$  depositados por evaporação e por deposição química em fase vapor,” *Revista Brasileira de Energia Solar*, vol. 7, pp. 1–7, 2016.